International Journal of Microwave and Wireless Technologies

cambridge.org/mrf

Trapezoidal pulse-switching strategy for failure correction of multi-pattern time-modulated linear array

Ananya Mukherjee, Sujoy Mandal, Sujit K. Mandal and Rowdra Ghatak

Microwave and Antenna Research Laboratory, Department of Electronics and Communication Engineering, National Institute of Technology Durgapur, Durgapur – 09, West Bengal, India

Research Paper

Cite this article: Mukherjee A, Mandal S, Mandal SK, Ghatak R (2023). Trapezoidal pulse-switching strategy for failure correction of multi-pattern time-modulated linear array. *International Journal of Microwave and Wireless Technologies* **15**, 1188–1204. https://doi.org/10.1017/S1759078722001179

Received: 9 May 2022
Revised: 1 October 2022
Accepted: 4 October 2022

Key words:
Differential evolution; pulse shaping; side lobe level; time modulated linear array

Author for correspondence:
Sujit K. Mandal,
E-mail: skmandal2006@gmail.com

Abstract

In this paper, a novel approach for simultaneously correcting multiple degraded patterns under the failure condition of time-modulated linear arrays is proposed. The approach is based on the use of trapezoidal pulse with non-zero rise/fall time to control the switching status of the radio frequency switches that enables ON-OFF keying modulation of the array elements. After deriving a closed form expression of harmonic power loss and through the in-depth analysis, it is explored that the proposed trapezoidal pulse, because of having non-zero rise/fall time, provides less undesired harmonic power loss as compared to the conventionally used rectangular pulse with ideally zero rise/fall time. With the aim of reconstructing the degraded patterns with improved directivity and suppressed higher sideband power, three pulse-switching strategies based on rectangular and trapezoidal pulse have been employed, and their comparative performances prove the superiority of the proposed approach.

Introduction

In the last two decades, time-modulated array (TMA) has received much attention to the antenna community because of its attractive features of realizing low/ultra-low sidelobe patterns with a cost-effective, simplified feed network [1, 2]. However, as an outcome of the periodic ON-OFF keying modulation of the excitation amplitude, the harmonic signals, also known as sideband radiations (SBR), appear in multiples of the modulation frequency [3, 4]. Initially, the harmonic radiation from TMA was considered as the undesired effect that leads to wastage of a part of the input power and reduces the directivity and overall radiation efficiency of the array [5]; thus successfully minimized [1, 6–8]. Toward this, a pulse-shaping strategy by considering non-ideal switch is also proposed in [9–12]. In the last decade, it is envisaged that the harmonics in TMA can be beneficially exploited to achieve multiple patterns simply by controlling the switching sequences [13–16]. The switching sequence define the elementwise switching state represented by different switching parameters such as on-time instant, on-time duration, rise time, fall time, off-time instant, and off-time duration. The multi-pattern TMAs are found to be useful in different communication systems such as cognitive radio [13], satellite communication [14], RADAR [15], and other telecommunication applications [16]. In the said applications, large antenna arrays are used, and the possibility of one or more element failure is quite a common phenomenon. Since multiple patterns at different harmonics are formed with the superposition of the signals from the individual array elements, the failure of an array element degrades significant amount of transmit power from the system. This deforms all the patterns produced by the array at both the center carrier frequency as well as at the harmonic frequencies. As a preventive measure, early identification of the failed or damaged elements and their replacement is essential. In this regard, the neural network [17], genetic algorithm (GA) [18], and differential evolution (DE) [19] based failure detection strategy are notable. However, the replacement of failed or damaged elements is not possible for the arrays used in satellites or in space applications. In such cases, instead of replacing the faulty elements, the deformed array pattern is reconfigured close to the original pattern by appropriately re-synthesizing the feeding distributions of the working array elements from the ground station [20, 21]. Toward the aim of reconfiguring the far-field pattern in conventional phase arrays (CPAs) by re-estimating the amplitude and phase distributions of the remaining active elements, several methods based on numerical techniques such as a conjugate gradient [22], sparse recovery [23], and stochastic optimization approaches using GA [24] and firefly algorithm [25] have been reported. Also, the potentiality of time-modulation (TM) to reconfigure the center frequency pattern in the presence of element failure is presented in [26, 27].

However, all failure correction methods reported so far have been proposed to reconfigure a single pattern and their performances to reconfigure multiple harmonic patterns need to be

© The Author(s), 2022. Published by Cambridge University Press in association with the European Microwave Association

explored. Usually, lower-order few harmonics are selected to synthesize the desired multiple patterns as the power at higher order harmonics are gradually diminished and become insignificant. In this regard, the Fourier spectrum of the pulse sequence used to modulate the static excitation plays an important role. The radiation performance by applying non-ideal rectangular pulse has been reported in [28, 29]. The ideal rectangular pulse with sharp transition (ideally zero rise/fall time) results a significant amount of power to be spread in the higher order harmonics [3]. Thus, failure correction of the harmonic power pattern using rectangular pulse is not efficient when power accumulation is an issue and the target is to minimize the undesired harmonic power loss. Therefore, to reconfigure multiple patterns with desired side lobe level (SLL), and directivity by simultaneously suppressing undesired power losses in the presence of element failure is a challenging task.

A close form expression of the total harmonic power by considering symmetric [3] and asymmetric [30] rectangular pulse has been reported. Also, the calculation of SBR for different TMA geometry and shaped pulses has been proposed in [31, 32]. To deal with multiple harmonic patterns by efficiently minimizing the loss through undesired harmonics, the SBR calculation has not being studied for asymmetrically positioned pulse with non-zero on-time instant, which is indispensable.

In this paper, a novel TM strategy using the trapezoidal pulse is proposed for the first time in the failure correction of multi-pattern TMA. The detailed analytical studies on the behavior of harmonic characteristics of rectangular and trapezoidal pulse have been presented. It is examined that the trapezoidal pulse shape with a gradual slope in the rise/fall time has better spectral characteristics, which distribute relatively lower power at higher order harmonics and higher power at lower order harmonics. Based on the rectangular and trapezoidal pulses, three pulse-shaping strategies as detailed in section "Numerical results and analysis" have been used for controlling the ON-OFF status of the switches. Through the comparative analysis of the reconfigured patterns, it is verified that the proposed trapezoidal pulse-based TM strategies exhibit better failure correction ability with improved directivity than the conventionally used rectangular switching scheme. The rest of the paper is organized as follows. The theory and problem formulation with χ set of element failure and its reconfiguration technique are described in section "Theory and problem formulation". Section "Numerical results and analysis" deals with detail numerical results and analysis showcasing the effectiveness of the proposed pattern reconfiguration method in dual beam time-modulated linear array (TMLA). Finally, conclusions are drawn in section "Conclusion".

Theory and problem formulation

The configuration of an N element symmetrically spaced TMLA is shown in Fig. 1. The array elements are assumed to be isotropic and uniformly spaced along X-axis with inter-element spacing d. The ON-OFF status of each array element is controlled by the respective RF switch, S_n: $(\forall n \in 1, N)$ connected with it. If the ON-OFF status of the n^{th} switch is controlled by using a periodic pulse sequence $U_n^{\Upsilon}(t)$, the array factor of such TMLA is expressed as [3],

$$AF(\theta, \phi, t) = e^{j2\pi f_0 t} \sum_{n=1}^{N} A_n e^{j\alpha_n} U_n^{\Upsilon}(t) e^{j(n-1)\beta d \sin\theta \cos\phi}, \quad (1)$$

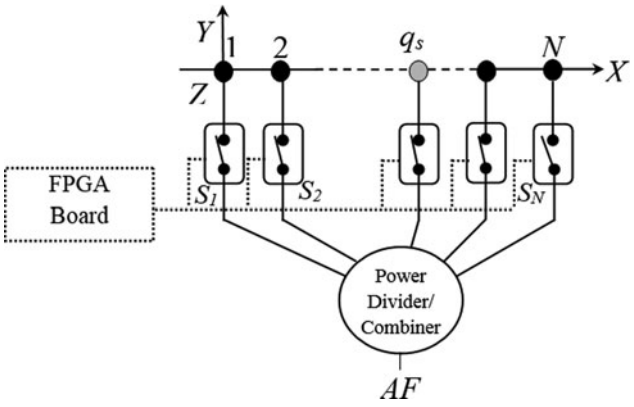


Fig. 1. N element time-modulated linear array in the presence of element failure, $\chi = \{q_1, q_2, \ldots, q_s\}$.

where f_0 is the operating carrier frequency of the antenna array; A_n and α_n are static excitation amplitude and phase of n^{th} element; β is the wave number; θ and $\phi$are the elevation and azimuthal angle measured from the broadside direction and X-axis respectively. Also, $Z_n = (n-1)d$ represents the coordinate of the n^{th} array element. The periodic switching function $U_n^{\Upsilon}(t)$ with time period T_P has the common periodic property of $U_n^{\Upsilon}(t) = U_n^{\Upsilon}(t)(t + \Gamma T_p)$, where Γ is a natural number. It should be mentioned here that, the superscript "Υ" is used here to denote any of the switching function while in the following sections "Υ" is replaced by the superscript "R" and "T" that represent rectangular and trapezoidal pulse-based modulation. Because of the periodicity of $U_n^{\Upsilon}(t)$ in time domain, different harmonic signals are generated at multiples of the modulation frequency, $f_p = 1/T_P$ surrounding the center carrier frequency as $f_0 \pm kf_p$. For the array with uniform static excitation, without loss of any generality, let us consider, $A_n = 1$: $(\forall n \in 1, N)$ and $\alpha_n = 0$: $(\forall n \in 1, N)$. Now, using Fourier series expansion in (1), the array factor expression at k^{th} harmonic in XZ plane $(\phi = 0^0)$ is obtained as,

$$AF_k(\theta, t) = e^{j2\pi(f_0 + kf_p)t} \sum_{n=1}^{N} a_{nk} e^{j\psi_n(\theta)}, \quad (2)$$

where a_{nk} is the complex Fourier coefficient for n^{th} element at k^{th} harmonic; and ψ_n is the progressive phase shift given by $\psi_n = z_n \beta \sin\theta$. Let the array contains a number of faulty elements and χ represents the set of "s" faulty elements as $\chi = \{q_1, q_2 . . q_j . . . q_s\}$; where $s \in [1, N]$ and q_s is the location of the faulty element as indicated in Fig. 1. Therefore, the time-independent array factor expression of the TMLA with χ set of faulty elements (AF_k^{χ}) can be represented as,

$$AF_k^{\chi}(\theta, t) = AF_k(\theta, t) - e^{j2\pi(f_0 + qf_p)t} \sum_{q \in \chi} a_{qk} e^{j\psi_q(\theta)}. \quad (3)$$

From (3), it can be seen that due to the presence of the faulty elements, the failure-free array factor differs from the failed array factor(AF_k^{χ}), i.e. $AF_k \neq AF_k^{\chi}$. As a result, a non-negligible difference at different sample positions of θ is obtained between the reference (AF_k) and failed (AF_k^{χ}) harmonic patterns.

https://doi.org/10.1017/S1759078722001179 Published online by Cambridge University Press

For the TMLA with $d = \lambda/2$, the directivity of the pattern at f_0 (D_0) and f_k (D_k) can be obtained as [5, 26],

$$D_0 = \frac{4\pi |AF_0(\theta, t)_{\max}|^2}{P_T} = \frac{4\pi \left|\sum_{n=1}^{N} \tau_n\right|^2}{P_T}, \tag{4}$$

$$D_k = \frac{4\pi |AF_k(\theta, t)_{\max}|^2}{P_T} = \frac{4\pi \left|\sum_{n=1}^{N} \tau_n \sin c(k\pi\tau_n)\right|^2}{P_T}, \tag{5}$$

where $P_T = P_{f0} + P_{SRk} + P_{SRH}$ is the total radiated power while P_{f0}, P_{SRk}, and P_{SRH} are the power at center frequency, power at desired harmonic frequency, and total sideband power including all undesired harmonics, respectively. Therefore, the sideband power P_{SR} ($= P_{SRk} + P_{SRH}$) radiated at both desired and undesired harmonics can be defined as below [3],

$$P_{SR} = \sum_{n=1}^{N} \left\{ |A_n|^2 \sum_{k=-\infty}^{\infty} a_{nk}^2 \right\} + 2 \sum_{\substack{m,n=1 \\ m \neq n}}^{N} \left\{ \mathrm{Re}\langle A_m A_n^* \rangle \sin c[\beta(z_m - z_n)] \sum_{k=-\infty}^{\infty} a_{mk} a_{nk}^* \right\}, \tag{6}$$

where m, n represent the index of all non-repeated set of the array elements present in the TMLA. In this regard, the overall system efficiency of TMLA (η_O) with SPST switches is the product of harmonic efficiency (η_H) and switching efficiency (η_S) [33, 34] as defined below,

$$\eta_H = \frac{\text{Power radiated at desired harmoincs } (P_D)}{\text{Total power radiated in all harmonics } (P_T)} = \frac{\sum_{k \in Z} P_k}{\sum_{k=-\infty}^{\infty} P_k}; \; Z \text{ is the desired set}, \tag{7}$$

$$\eta_s = \frac{\text{Total output power from TMA } (P_T)}{\text{Input power fed to the array } (P_{in})} = \frac{\sum_{k=-\infty}^{\infty} P_k}{N}. \tag{8}$$

It is observed from (4) and (5) that, P_{SR} radiated at both desired and undesired harmonics appeared in the denominator of the directivity expressions. In addition to that the χ set of faulty elements reduce the maximum obtainable power of the respective radiation patterns. Thus, both the undesired harmonic power and number of faulty elements reduce the overall system efficiency (η_O) and the directivity of the reconfigured patterns.

Under failure condition of the array, to correct or reconfigure the degraded array patterns simultaneously at $k = 0$ and $k \neq 0$, the conventionally used rectangular pulse, $U_n^R(t)$ for which rise/fall time is zero and trapezoidal pulse $U_n^T(t)$ for which rise/fall time is non-zero are used to modulate the array elements. For failure correction application, the suitability of using the switching pulses with various rise/fall times has been analyzed and investigated in the following sections.

Conventional rectangular pulse

The shifted rectangular switching pulse $U_n^R(t)$ over a modulation period as pictorially represented in Fig. 2(a) is mathematically defined as,

$$U_n^R(t) = \begin{cases} 1 & t_{on} \leq t \leq t_{on} + \tau_n \leq Tp \\ 0 & else \end{cases}. \tag{9}$$

In (9), t_{on} and τ_n are the two parameters of the pulse used to control the ON-time instant (OTI) and ON-time duration (OTD) of the switch. Representing their normalized values as $\xi_n = \tau_n/T_p$ and $\vartheta_n = t_{on}/T_p$, the spectral component of the rectangular pulse can be obtained from Fourier coefficient, a_{nk}^R and is

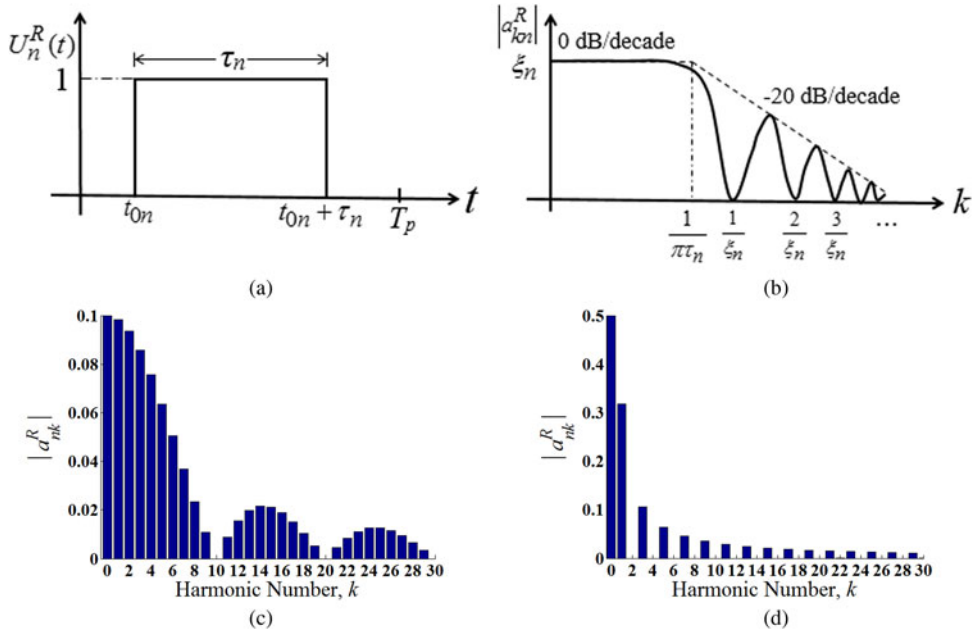


Fig. 2. The behavior of the rectangular switching function. (a) Time domain switching waveform. (b) Spectral bound and envelop. (c) Harmonics for $\xi_n = 0.1$. (d) Harmonics for $\xi_n = 0.5$.

https://doi.org/10.1017/S1759078722001179 Published online by Cambridge University Press

expressed as [16],

$$a_{nk}^{R}(\xi_n, \vartheta_n) = \xi_n \frac{\sin(k\pi\xi_n)}{k\pi\xi_n} e^{-jk\pi(\xi_n+2\vartheta_n)}. \quad (10)$$

It can be seen from (2) and (10) that, depending on the value of ξ_n, the harmonic coefficient of the n^{th} time-modulated element will contribute to produce the resultant k^{th} order sideband pattern.

For a given value of ξ_n, the envelope of the harmonic spectrum with the harmonic indices is depicted in Fig. 2(b). As expressed in (10), the harmonic coefficient is in the form of $sinc(x) = sin(x)/x$, where $x = k\pi\xi_n$. Therefore, the approximated upper bound of the $|a_{nk}^{R}|$ can be obtained from the bode plot of two linear asymptotes with slope of 0 and −20 dB/decade as shown with the dotted line in Fig. 2(b) [35]. It is to be noted that, the corner frequency $f_{c1} = (1/\pi\tau_n) = (1/\pi T_p)(T_p/\tau_n) = (1/\pi\xi_n)f_p$ is inversely related to the duty cycle of the pulse. This provides the useful information that the radiated harmonic signal power starts to decrease at the rate −20 dB/decade after the harmonic order $k > (1/\pi\xi_n)$. The harmonic spectrums ($\forall k \in (1, 30)$) of a rectangular pulse with normalized on-time durations, i.e. duty cycles, $\xi_n = 0.1$ and 0.5 are shown in Figs 2(c) and 2(d). It can be seen from (10) that $|a_{nk}^{R}|$ is equal to zero at $k = m/\xi_n$, $\forall m \in \mathbb{Z} \wedge \neq 0$. As a result, with the value of $\xi_n = 0.1$, the magnitude of the harmonic coefficient becomes zero at harmonic order $k = \pm 10$ m, i.e. at harmonic frequencies $\pm f_{10}$ $(=f_0 \pm 10f_p)$, $\pm f_{20}$, $\pm f_{30}$ as in Fig. 2(c). Similarly, for $\xi_n = 0.5$, no radiation occurs at frequencies $\pm f_k = f_0 \pm kf_p$; where $k = \pm 2m$ (Fig. 2(d)). Thus, the spectrum characteristics indicate that, by proper selection of the set of on-time sequence ξ_n, the overall higher order harmonic power, P_{SR}^{R} generated by the shifted rectangular pulse (Fig. 2(a)) as defined in (11) and (12) [36] can be reduced to improve the directivity while at the same time, the same set of on-time sequence can generate the desired power pattern at the lower order harmonics.

$$P_{SR}^{R} = 2\pi \sum_{n=1}^{N} |A_n|^2 \xi_n^R (1 - \xi_n^R) + 2\pi \sum_{\substack{m,n=1 \\ m \neq n}}^{N} \Re\{A_m A_n^*\}[\overline{\xi_{mn}^R} - \xi_m^R \xi_n^R] sinc[\beta(z_m - z_n)], \quad (11)$$

where $\overline{\xi_{mn}^R}$ is the intersected on-time duration of the rectangular pulse [36]. Whereas for $d = \lambda/2$ uniformly exited TMLA having $\xi_m^R = \xi_n^R$ the expression of P_{SR}^{R} becomes,

$$P_{SR}^{R} = 2\pi \sum_{n=1}^{N} \xi_n^R (1 - \xi_n^R). \quad (12)$$

Trapezoidal pulse

A trapezoidal switching function, $U_n^T(t)$ as shown in Fig. 3(a) is mathematically represented as

$$U_n^T(t) = \begin{cases} t/\Delta_n & t_{0n} \le t \le t_{0n} + \Delta_n \\ 1 & t_{0n} + \Delta_n \le t \le t_{0n} + \Delta_n + \tau_n \\ -t/\Delta_n & t_{0n} + \Delta_n + \tau_n \le t \le t_{0n} + 2\Delta_n + \tau_n \le T_p \\ 0 & else. \end{cases} \quad (13)$$

The pulse is defined with three parameters – OTI → t_{0n}, and OTD → τ_n as defined for rectangular pulse and one additional parameter, namely, rise/fall time → Δ_n. In terms of the normalized values of OTI → $\vartheta_n = (t_{on}/T_p)\, t/\Delta_n$, OTD → $\xi_n = \tau_n/T_p$, and rise/fall time → $\delta_n = \Delta_n/T_p$; the complex Fourier coefficient (a_{nk}^{T}) of $U_n^T(t)$ can be obtained as in [35, 37],

$$a_{nk}^{T}(\xi_n, \vartheta_n, \delta_n) = \xi_n \frac{\sin(k\pi\xi_n)}{k\pi\xi_n} \frac{\sin(k\pi\delta_n)}{k\pi\delta_n} e^{-jk\pi(\xi_n+2\vartheta_n+\delta_n)}. \quad (14)$$

The envelop behavior of the spectrum characteristics (a_{nk}^{T}) of a trapezoidal pulse is shown in Fig. 3(b). It shows the dependency of higher order harmonics on Δ_n along with τ_n. As compared to the rectangular pulse, the non-zero rise/fall time in trapezoidal pulse leads to include another *sinc* function and hence the expression of the harmonic coefficient in (14) consists of the product of two *sinc* functions. As a result, an additional asymptote appears at the higher order harmonics after the second corner frequency $f_{c2} = 1/\pi\Delta_n$ with a slope of −40 dB/decade. Thus, the magnitude of the harmonic coefficient for the trapezoidal pulse will be less than that of the rectangular pulse, specifically at higher order harmonics. With $\xi_n = 0.5$ and normalized rise/fall time, $\delta_n (= \Delta_n/T_p) = 0.2$, the harmonic spectrum of the pulse is shown in Fig. 3(c). It can be seen from (16) that in addition to the harmonic order $k = (m/\xi_n)$ as in rectangular pulse, the coefficient of the trapezoidal pulse $(|a_{nk}^{T}|)$ also becomes zero at $k = m/\delta_n$. Thus, when $\xi_n = 0.5$ and $\delta_n = 0.2$, the harmonic coefficients are zero not only at $k = \pm 2m$ but also for $k = \pm 5$ m. As a result, in addition to the harmonic frequencies $\pm f_2, \pm f_4, \pm f_6, \ldots$ as for the case of rectangular

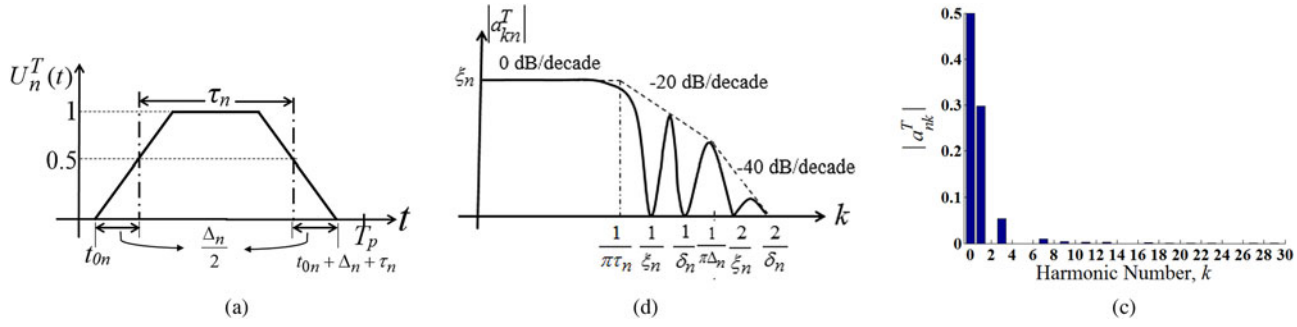


Fig. 3. Behavior of the trapezoidal switching function. (a) Time domain switching waveform. (b) Spectral bound and envelop. (c) Harmonics for $\xi_n = 0.5$, $\delta_n = 0.2$.

https://doi.org/10.1017/S1759078722001179 Published online by Cambridge University Press

pulse with $\xi_n = 0.5$, for the trapezoidal pulse with $\delta_n = 0.2$ harmonic radiations become zero at $\pm f_5$, $\pm f_{10}$, $\pm f_{15}$ … as appeared in Fig. 3(c). A closed form expression of the overall harmonic power of the proposed antenna array controlled by shifted trapezoidal pulse can be derived by using (6) and (14) as given below [9, 30] (Appendix I),

$$P_{SR}^{T} = 2\pi \sum_{n=1}^{N} |A_n|^2 \left[\xi_n^T (1 - \xi_n^T) - \frac{\delta_n^T}{3} \right] + 2\pi \sum_{\substack{m,n=1 \\ m \neq n}}^{N} \Re\{A_m A_n^*\} \left[\overline{\xi_{mn}^T} - \xi_m^T \xi_n^T - \frac{\overline{\delta_{mn}^T}}{3} \right] Sinc[\beta(z_m - z_n)], \tag{15}$$

where $\overline{\xi_{mn}^R}$ and $\overline{\delta_{mn}^T}$ are the intersected on-time duration and rise/fall time duration of two consecutive trapezoidal pulses, respectively. For the similar condition, $A_n = 1$, $d = \lambda/2$, $\xi_m^T = \xi_n^T$, and $\delta_m^T = \delta_n^T$, (15) can be reduced to as given below,

$$P_{SR}^{T} = 2\pi \sum_{n=1}^{N} \left[\xi_n^T (1 - \xi_n^T) - \frac{\delta_n^T}{3} \right]. \tag{16}$$

Therefore, the higher order harmonics generated using trapezoidal pulse is expected to be less as compared to the rectangular pulse.

Conventional rectangular versus trapezoidal pulse

From the above analysis, a comparative performance in term of power spectral characteristics of the two pulses at higher order harmonics can be realized. It is to be noted that a rectangular pulse becomes trapezoidal with the non-zero value of rise/fall time. To get a clear picture about the spectral characteristics, for the pulse of fixed values of $\xi_n = 0.5$, 0.3, and 0.2; the Fourier coefficients for different values of $\delta_n = 0.1$, 0.2, 0.3 are plotted in Figs 4(a)–4(c). By comparing the spectral characteristics, it can be observed that for different δ_n, the Fourier coefficients at $k = 0$ remain same. This is because, the coefficient at $k = 0$ depends on the area of the pulse while the area of the trapezoidal pulse doesn't change with δ_n due to its symmetric shape. Further, it is evident from the spectrum that compared to the higher harmonics, the effect of increasing δ_n on lower harmonic coefficients is less. Since the coefficient of the trapezoidal pulse at higher harmonic order is drastically decreased, pattern synthesis at lower harmonic using trapezoidal pulse as the time-modulating signal not only provides less higher harmonic power loss, it also offers an additional control parameter or flexibility in terms of rise/fall time of the pulse to synthesize the desired patterns at lower harmonics. It is to be noted that the modern function generator features to provide various pulse shapes with independently controllable rise and fall time (https://www.valuetronics.com/pub/media/vti/datasheets/Wavetek%20166.pdf). However, the modulating trapezoidal pulsed waveforms with desired rise/fall time can be controlled by programming the FPGA board as indicated in Fig. 1.

Failure correction

Already it is mentioned that under the failure condition, the new set of pulse sequences is used to reproduce the degraded harmonic patterns at the desired lower order harmonics while the higher order harmonic power is suppressed significantly. If, for the case of rectangular pulse-based TM, the set of switching parameters required to correct the degraded harmonic patterns is $\xi^c = \{\xi_n^c | \forall n \in (1, N) \wedge n \notin \chi\}$ and $\vartheta^c = \{\vartheta_n^c | \forall n \in (1, N) \wedge n \notin \chi\}$; the corresponding array factor, $AF_k^{Rc}(\theta, t)$ of the corrected pattern at k^{th} order harmonic is expressed as

$$AF_k^{Rc}(\theta, t) = e^{j2\pi(f_0 + kf_p)t} \sum_{n=1, n \neq \chi}^{N} \xi_n^c \frac{\sin(k\pi\xi_n^c)}{k\pi\xi_n^c} e^{-jk\pi(\xi_n^c + 2\vartheta_n^c)} e^{j\psi_n}. \tag{17}$$

Similarly, for the trapezoidal pulse switching, if the set of the switching parameters of the corrected patterns is ($\xi^c = \{\xi_n^c | \forall n \in (1, N) \wedge n \notin \chi\}$; $\vartheta^c = \{\vartheta_n^c | \forall n \in (1, N) \wedge n \notin \chi\}$;and $\delta^c = \{\delta_n^c | \forall n \in (1, N) \wedge n \notin \chi\}$); the corresponding corrected array factor expression, $AF_k^{Tc}(\theta)$ is given as,

$$AF_k^{Tc}(\theta, t) = e^{j2\pi(f_0 + kf_p)t} \sum_{n=1, n \neq \chi}^{N} \xi_n^c \frac{\sin(k\pi\xi_n^c)}{k\pi\xi_n^c} \frac{\sin(k\pi\delta_n^c)}{k\pi\delta_n^c} e^{-jk\pi(\xi_n^c + \delta_n^c + 2\vartheta_n^c)} e^{j\psi_n}. \tag{18}$$

Under the failure condition, the set switching parameters corresponding to the utilized switching pulse are properly tuned to correct the distorted patterns. To determine the optimum switching parameters for the corrected array patterns ($AF_k^{\Upsilon c}(\theta, t)$; $\Upsilon = R, T$) at $k = 0$ and closed to the desired reference

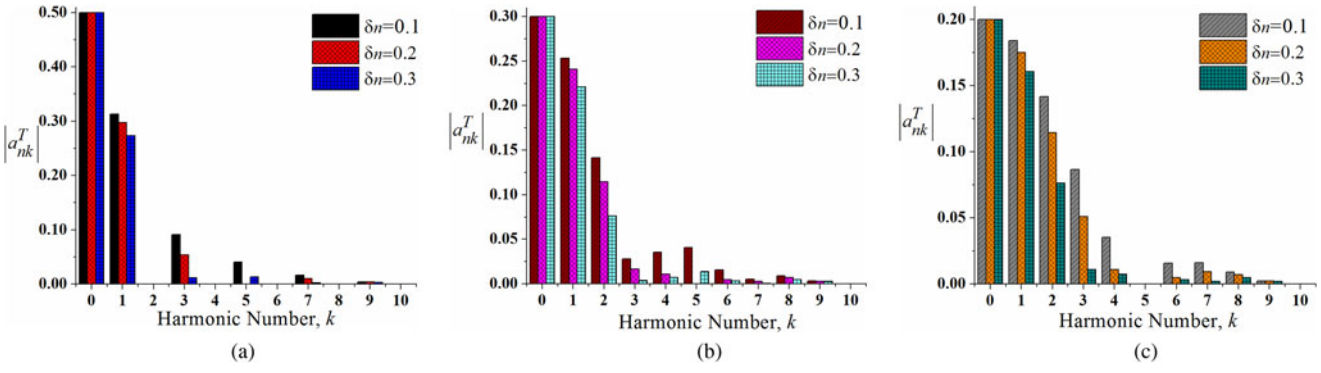


Fig. 4. Comparison of harmonic coefficients under different values of the pulse-shaping parameters. (a) $\xi_n = 0.5$, (b) $\xi_n = 0.3$, (c) $\xi_n = 0.2$.

https://doi.org/10.1017/S1759078722001179 Published online by Cambridge University Press

pattern ($AF_k^{\mathrm{Ref}}(\theta, t)$), the global search evolutionary optimization algorithm namely, DE [38, 39] with DE/rand/1/bin strategy is used. To realize the patterns, the cost function is defined as

$$f^g(\mu^{\mathrm{Y}})_{\mathrm{Y}=R,T} = \sum_{k=\mathrm{Z}} \left\{ \sum_{\zeta=\{\zeta_{\mathrm{Z}}\}} w_{\zeta_{\mathrm{Z}}} \cdot H\{\Omega_{\zeta_{\mathrm{Z}}}(\mu^{\mathrm{Y}})\}.|\Omega_{\zeta_{\mathrm{Z}}}(\mu^{\mathrm{Y}})| \right\}. \quad (19)$$

Here, g represents the iteration index of the iterative evolutionary algorithm; μ^{Y} represents the optimization parameter vector. For rectangular pulse-switching modulation, it is given as $\mu^R = \{\xi^c, \vartheta^c\}$, while for trapezoidal pulse-switching modulation, it is $\mu^T = \{\xi^c, \vartheta^c, \delta^c\}$. In (19), Z is the set of harmonic number at which multiple patterns are realized and ζ_{Z} is the set of parameters associated with the synthesized pattern at a particular harmonic. For example, if a sum pattern is synthesized only at fundamental (center) frequency ($k = 0$) then Z→{0} and $\zeta_0 = \{SLL_0, FNBW_0, D_0\}$. However, if multiple patterns are synthesized at fundamental ($k = 0$) and at first harmonic ($k = 1$), then Z→{0, 1} and ζ_{Z}represents the corresponding radiation parameters of the patterns to be optimized. As per example, suppose two narrow beam sum patterns are generated both at $k = 0$ and 1 then the associated radiation parameters of the corresponding harmonic patterns to be optimized (ζ_{Z}) are respectively given as $\zeta_0 = \{SLL_0, FNBW_0, D_0\}_{sum}$, $\zeta_1 = \{SLL_1, FNBW_1, D_1, SBL_1, SBL_{\max}\}_{sum}$; where SBL_1 and SBL_{max} represent sideband level at first harmonic and the value of maximum sideband level among the higher harmonics respectively. H (.) is the Heaviside step function.

If, in addition to the sum pattern at fundamental, a wide beam flat top pattern is generated at $k = 1$; then the corresponding radiation parameters related to the first harmonic are written as $\zeta_1 = \{SLL_1, FTBW_1, ripple, SBL_1, SBL_{\max}\}_{flat-top}$. $\Omega_{\zeta_{\mathrm{Z}}} = (\zeta_{\mathrm{Z}} - \zeta_{\mathrm{Z}d})$, where $\zeta_{\mathrm{Z}d}$represents the desired values of the radiation parameters. $w_{\zeta_{\mathrm{Z}}}$ is the corresponding weighting factor. This is a minimization problem where minimization of the cost function leads to reconfigure the pattern toward the desired one in terms of the required radiation characteristics.

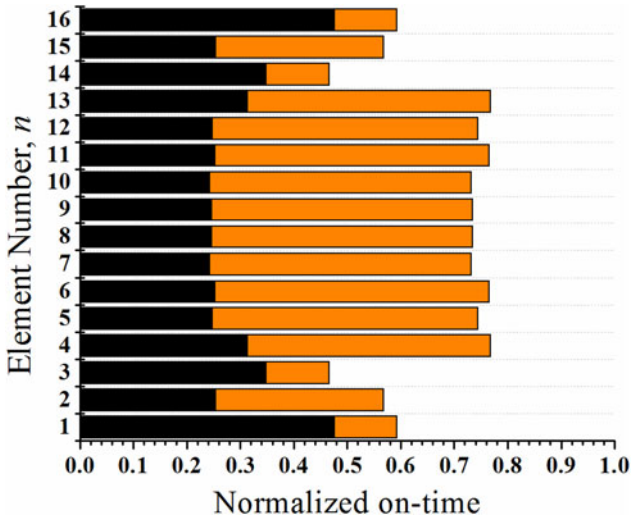


Fig. 5. DE-optimized element-wise pulse-switching sequence to synthesize the sum-sum pattern for a TMLA of $N = 16$ (Example 1).

Table 1. Radiation performance of TMLA of $N = 16$, $d = \lambda/2$ (Example (1))

		f_0				f_1			P_{SR}%				
	Array status	SLL_0 (dB)	$FNBW_0$ (deg)	D_0 (dBi)	SBL_1 (dB)	SLL_1 (dB)	$FNBW_1$ (deg)	D_1 (dBi)	SBL_{max} (dB)	P_{f0}%	P_{SR1}	P_{SRH}	η_H %	η_S%	η_T %
Cases	Failure free: $\chi = 0$	−19.76	19.17	18.79	−3.43	−19.31	18.21	15.65	−20.03	44.48	40.58	14.92	85.07	37.00	31.48
Case1	Failure with $\chi = \{5\}$	−14.13	20.65	18.42	−3.39	−13.90	23.23	15.34	−19.27	43.99	40.52	15.47	84.53	33.92	28.68
	Corrected i. $\delta_n^c = 0$	−19.63	22.35	18.01	−2.89	−18.71	19.53	15.14	−17.84	42.47	40.82	16.69	83.30	32.91	27.41
	ii. δ_n^c = uniform	−19.65	22.69	19.26	−3.98	−18.77	19.14	15.34	−19.82	55.55	41.38	3.07	96.93	30.95	29.82
	ii. δ_n^c = variable	−19.27	20.30	19.00	−3.55	−19.47	18.66	15.50	−20.71	50.12	40.48	9.40	91.60	32.29	29.58
Case2	Failure with $\chi = \{2,13\}$	−15.24	29.94	18.27	−3.43	−12.77	25.28	15.03	−20.42	45.15	39.98	14.85	85.14	32.24	27.45
	Corrected i. $\delta_n^c = 0$	−19.62	25.16	17.72	−3.00	−19.18	22.75	14.70	−19.11	43.70	41.59	14.70	85.30	32.96	28.11
	ii. δ_n^c = uniform	−19.16	24.53	19.45	−3.44	−18.86	22.38	14.89	−20.08	48.34	41.50	6.81	89.85	33.30	29.92
	ii. δ_n^c = variable	−19.46	22.12	18.69	−3.20	−19.27	21.01	14.14	−19.31	47.30	41.28	11.42	92.59	31.49	29.15

https://doi.org/10.1017/S1759078722001179 Published online by Cambridge University Press

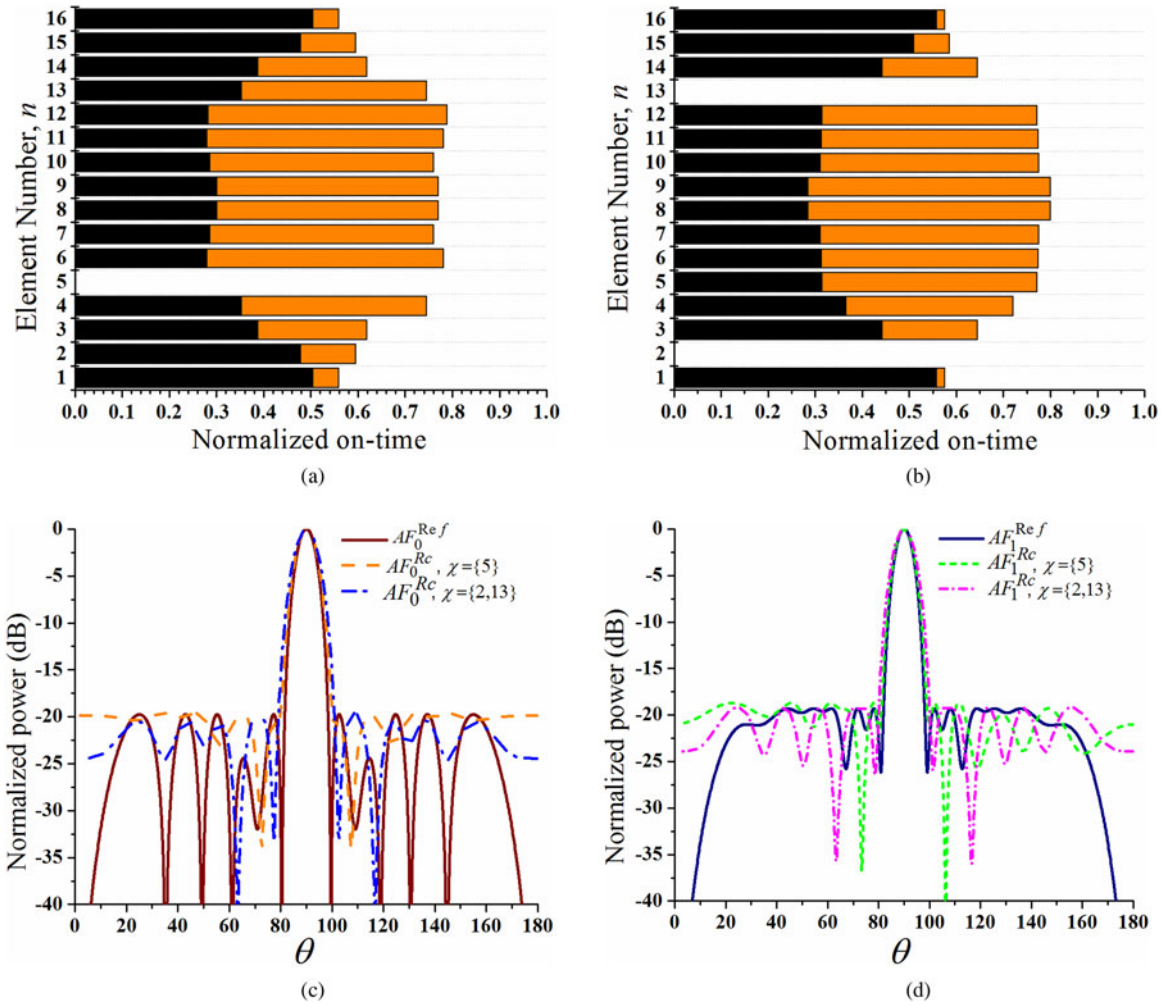


Fig. 6. DE-optimized corrected pulse-switching sequence and synthesized sum-sum patterns for a TMLA of $N = 16$ (Example 1) using rectangular pulse with zero rise/fall time ($\delta_n^c = 0$). (a) Element-wise switching sequences with a set of faulty elements, $\chi = \{5\}$ and (b) $\chi = \{2, 13\}$, (c) normalized radiation patterns at f_0, and (d) normalized radiation patterns at f_1.

Numerical results and analysis

To verify the concept of the analysis made in the previous sections, regarding the superiority of using trapezoidal pulse over rectangular pulse, the comparative results of two examples are presented. In the first example, a dual-beam TMLA ($N = 16$, $d = 0.5\lambda$) of sum-sum patterns at the center carrier frequency (f_0) and first harmonic (f_1) is considered. In the second example, to show the versatility of correcting the diverse shape of patterns, another dual-beam TMLA ($N = 32$, $d = 0.5\lambda$), producing sum pattern at f_0 and flat-top pattern at f_1 is taken. In both examples, the number elements are selected the same as considered in the two examples in [24] wherein rectangular pulse-based switching is used to correct the failure of a single pattern at f_0. To synthesize the said reference patterns as well as to reconfigure the failure patterns, the tuning parameters of the MATLAB^{TM} coded DE optimization algorithm are set as population size (NP) = 50, mutation constant (η) = 0.4, and crossover probability (F) = 0.8. In the first example, for both of the dual patterns, the desired values of the radiation parameters are set in the cost function in (19) as $SLL_d = -20$ dB, $FNBW_d = 15^0$, $D_d = 15$ dBi, $SBL_{1-d} = -3$ dB, and $SBL_{max-d} = -20$ dB. In the second example, the desired criterion for the sum pattern is kept the same as in the first example. However, for the flat-top pattern, the desired values of the radiation parameters are selected as $SLL_d = -20$ dB, maximum ripple factor, $R_d = 0.5$ dB, and flat-top beam-width ($FTBW$) = 45°. To reconfigure the failure patterns, three different switching strategies have been imposed as (i) rectangular pulse with zero rise/fall time ($\delta_n^c = 0$); (ii) trapezoidal pulse of uniform rise/fall time, i.e. same $\delta_n^c (= \delta_0^c \neq 0)$ for all time-modulating elements; and (iii) trapezoidal pulse of non-uniform rise/fall time, i.e. different δ_n^c for the individual time-modulating elements. The performances of the different switching schemes to reconfigure the degraded patterns are tested under two cases of failure conditions – case 1: single-element failure and case 2: two-element failure. For the switching scheme in (i), ξ_n^c and ϑ_n^c are perturbed in the search range of [0.01, 1]. For the switching scheme in (ii) and (iii), the search range of ξ_n^c and ϑ_n^c are kept as [0.01, 1]; however, δ_n^c is varied in the range of [0.01, 0.2] such that the condition $(\xi_n^c + \vartheta_n^c + \delta_n^c) \leq 1$ is maintained to avoid the pulse duration longer than modulation period.

Example 1: failure correction of dual beam TMLA with sum-sum pattern

The DE-optimized switching sequence for the synthesized failure-free reference pattern is shown in Fig. 5. The different radiation

https://doi.org/10.1017/S1759078722001179 Published online by Cambridge University Press

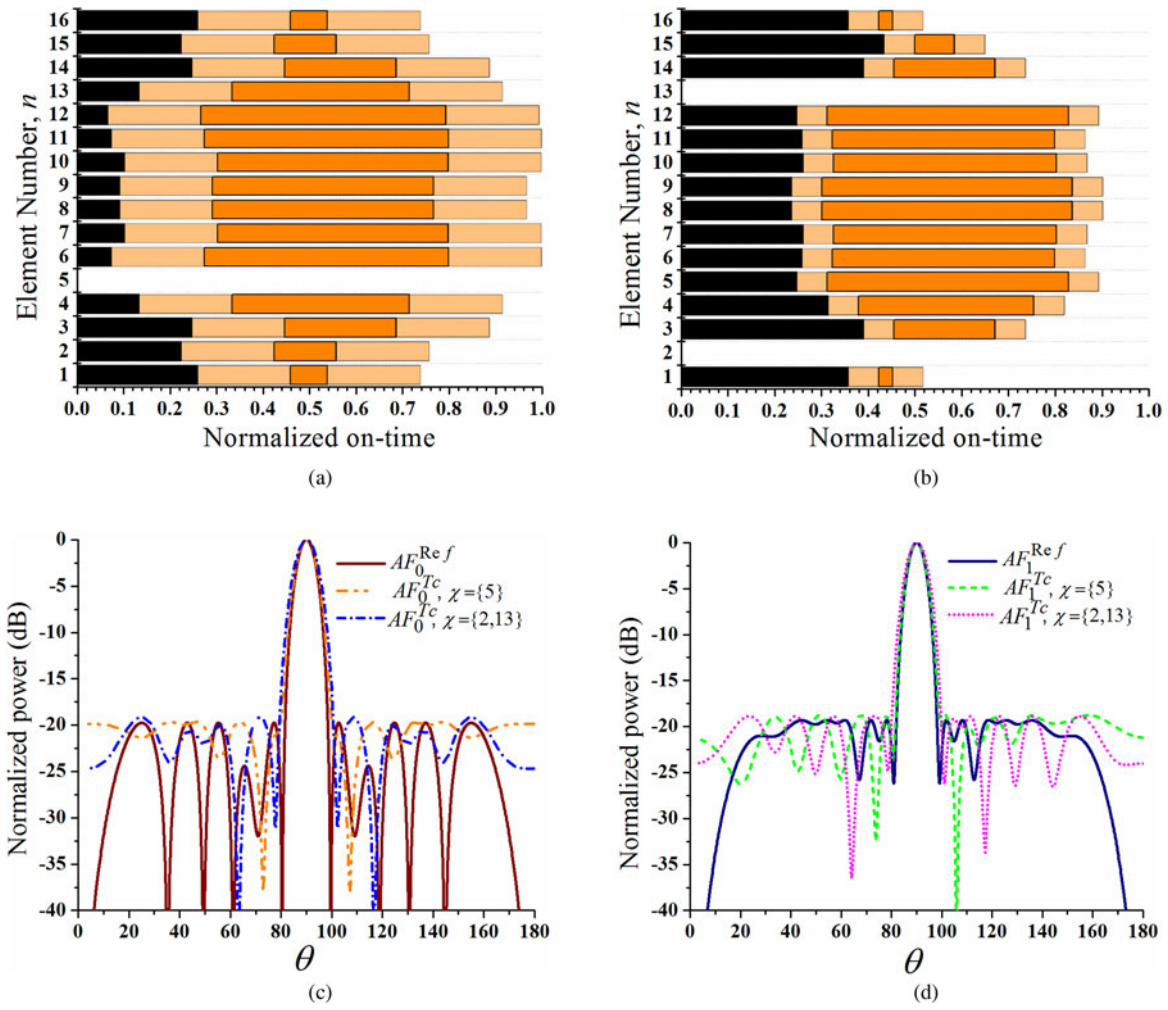


Fig. 7. DE-optimized corrected pulse-switching sequence and synthesized sum-sum patterns for a TMLA of $N = 16$ (Example 1) using trapezoidal pulse with uniform rise/fall time ($\delta_n^c = \delta_0^c$). (a) Element-wise switching sequences with $\chi = \{5\}$ and (b) $\chi = \{2, 13\}$, (c) normalized radiation patterns at f_0, and (d) normalized radiation patterns at f_1.

parameters for the synthesized failure-free patterns at f_0 and f_1 and the distorted patterns under the two cases of failure conditions of $\chi = \{5\}$ and $\chi = \{2, 13\}$ are listed in Table 1. It can be observed that a single element failure in case 1 seriously distorts both the carrier frequency and first harmonic frequency patterns. The reference SLLs (SLL_0 and SLL_1) and FNBWs ($FNBW_0$ and $FNBW_1$) corresponding to the patterns at f_0 and f_1 are respectively increased by (5.63 and 5.41 dB) and (1.48 and 5.02°) respectively. Similarly, under case 2, the SLLs and FNBWs of the reference patterns are degraded respectively by (4.52 and 6.54 dB) and (10.77 and 7.07°). Table 1 also shows that under failure conditions, due to the reduction of active elements, as compared to case 1, the directivity and overall system efficiency of both the patterns are decreased more in case 2.

Failure correction using rectangular pulse

To correct the deformed dual patterns under case 1 and case 2, at first, the conventional rectangular pulse-switching-based TM is used to the remaining active elements of the array. The DE-optimized switching parameters, $\mu^R = \{\xi_n^c, \vartheta_n^c\}$; $n \notin \{5\}$ for case 1 and $n \notin \{2, 13\}$ for case 2; of the corrected patterns are depicted in Figs 6(a) and 6(b) while the corresponding reconstructed patterns are shown in Figs 6(c) and 6(d) respectively. The radiation parameters of the corrected patterns under both cases are given in Table 1. The table shows that, for case 1, the SLLs of the reconfigured patterns are obtained as $SLL_0 = -19.63$ dB and $SLL_1 = -18.51$ dB, which are 0.13 and 0.80 dB higher than that for the reference SLLs of −19.76 and −19.31 dB, respectively. The FNBWs of the patterns at f_0 and f_1 are respectively increased by 1.18 and 1.32° and the directivities are decreased by 0.77 and 0.51 dBi. For the corrected pattern, the maximum value of the undesired higher order SBR, SBL_{max} is 2.19 dB higher than that of the reference pattern. With respect to the total power radiated by the array, the percentage of power radiated at $f_0 \rightarrow P_{f0}$; $f_1 \rightarrow P_{SR1}$ $(= \{\sum_{n=1}^{N} \xi_n^R Sinc(\pi \xi_n^R)\}^2)$ and in the remaining higher harmonics $\rightarrow P_{SRH}$ $(P_{SRH} = P_{SR} - P_{SR1})$ is also calculated, and their values are mentioned in Table 1. It can be seen that P_{f0} is reduced by 2.01%, while P_{SRH} is increased by 1.77%, and these lead to reduce the directivity of the patterns.

For case 2, the achieved SLLs ($SLL_0 = -19.62$ dB and $SLL_1 = -19.18$ dB) of the reconfigured patterns are closed to the failure-free reference patterns. However, FNBWs are increased by 6.01 and 4.54°, and the directivities are decreased by 1.07 and 0.95 dBi, respectively. Also, the reconfigured array pattern provides relatively higher values of SBL_{max} −19.11 dB. Further, the reduction of P_{f0} from 44.48 to 43.70% reduces the directivity D_0 by

https://doi.org/10.1017/S1759078722001179 Published online by Cambridge University Press

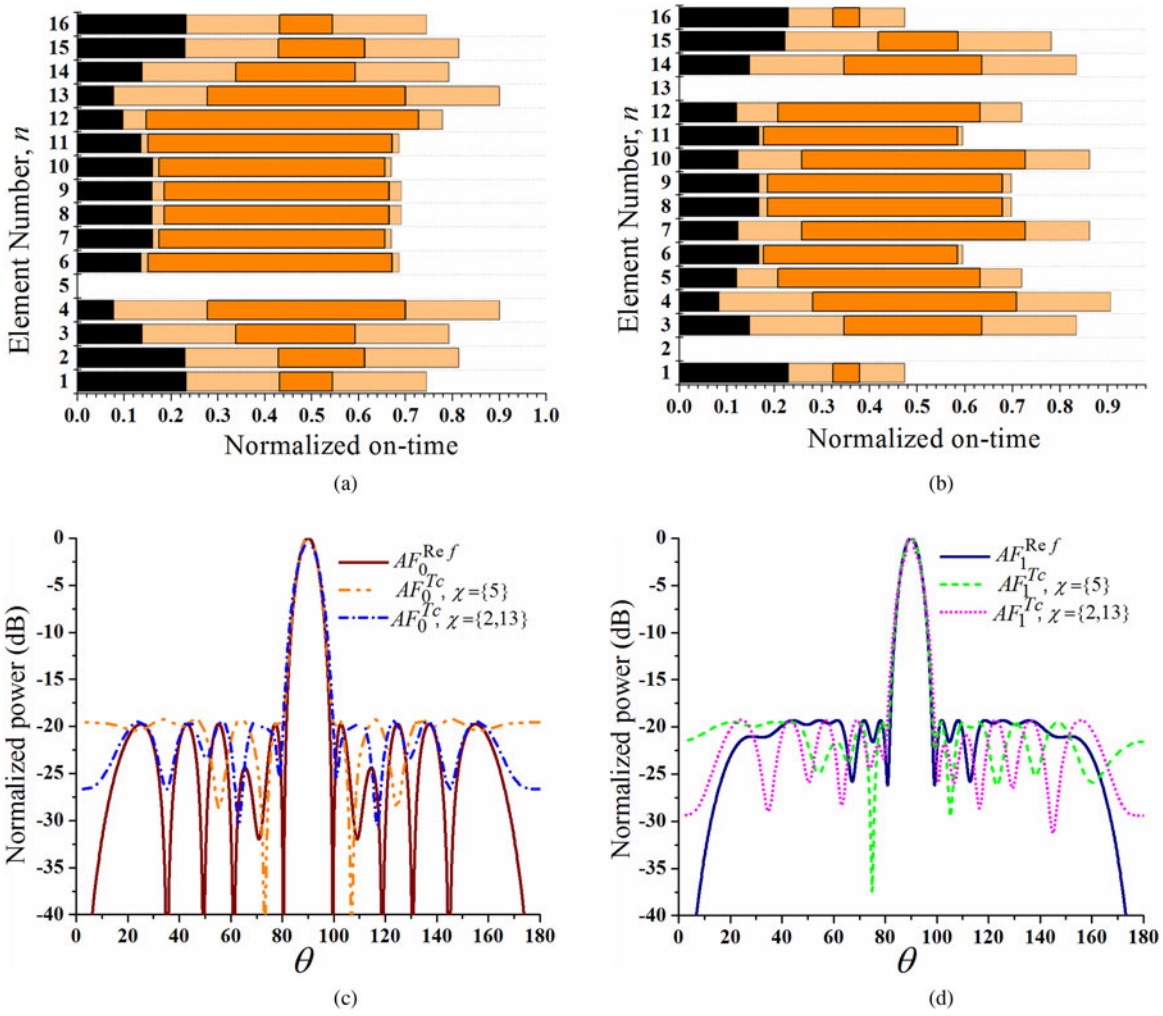


Fig. 8. DE-optimized corrected pulse-switching sequence and synthesized sum-sum patterns for a TMLA of $N = 16$ (Example 1) using trapezoidal pulse of variable rise/fall time δ_n^c. (a) Element-wise switching sequences with $\chi = \{5\}$, and (b) $\chi = \{2, 13\}$, (c) normalized radiation patterns at f_0, and (d) normalized radiation patterns at f_1.

1.07 dB_i. With respect to the failure condition, the efficiency only improved by 0.66%. This theoretical aspect is also mentioned in section "Conventional rectangular pulse", and the same is reflected in the result in Table 1 under both cases of the array failure. Thus, using conventional rectangular pulse-based modulation, it is much difficult to achieve the directivities of the patterns with the same values as that in reference patterns by simultaneously maintaining the low SLLs.

Failure correction using trapezoidal pulse with uniform rise/fall time

Now, to correct the degraded dual-beam patterns of the array under consideration, trapezoidal pulse-switching-based TM is employed. In this case, all modulating pulses are assumed to have uniform rise/fall time, such that $\delta_n^c = \delta_0^c; \forall n \in (1, N)$; where δ_0^c is the optimum value of the rise/fall time of the pulse. Thus, along with ξ_n^c and ϑ_n^c, δ_0^c considered as the optimization parameters and the corresponding unknown parameter vector becomes $\mu^T = \{\xi_n^c, \vartheta_n^c, \delta_0^c\}$. The obtained DE-optimized new set of switching parameters of the corrected patterns is depicted in Figs 7(a) and 7(b), and the corresponding reconstructed dual-beam patterns are shown in Figs 7(c) and 7(d), respectively. The figures show that the trapezoidal pulse with uniform non-zero rise/fall time successfully rebuilds the degraded patterns closed to the original one. The calculated radiation parameters of the reconfigured patterns are mentioned in Table 1. These results show that under two failure conditions, the trapezoidal pulse approach significantly reduces P_{SRH} from 15.47 and 14.85% to only 3.07 and 6.81%, respectively. These are less by 13.62 and 7.89% to the conventional rectangular pulse switching. These reduced P_{SRH} lead to an increase of P_{f0} to 55.55 and 48.34%, respectively, while $P_{SR1} = \{\sum_{n=1}^{N} \xi_n^T Sinc(\pi\xi_n^T) Sinc(\pi\delta_n^T)\}^2$ almost remains the same. As a result, the directivity (D_0) at f_0 is improved for both the cases of failure correction. The directivities of the corrected dual-beam patterns are calculated and are obtained as 19.26 and 15.34 dB for case 1; and 19.45 and 14.89 dB for case 2, respectively. These values indicate that the directivity of the trapezoidal pulse-based reconfigured patterns is higher than the respective reconfigured patterns as obtained using conventional rectangular pulse-based TM. Even, the directivity of the corrected patterns is higher than the failure-free patterns as synthesized by using the traditional rectangular pulse-based TM. Hence, with the inclusion of an additional degree of freedom δ_n^c along with ξ_n^c and ϑ_n^c, the deformed patterns

https://doi.org/10.1017/S1759078722001179 Published online by Cambridge University Press

https://doi.org/10.1017/S1759078722001179 Published online by Cambridge University Press

Table 2. Impact of faulty element position on radiation pattern characteristics

Cases	Array status		f_0			f_1						P_{SR}%				
			SLL_0 (dB)	$FNBW_0$ (deg)	D_0 (dBi)	SBL_1 (dB)	SLL_1 (dB)	$FNBW_1$ (deg)	D_1 (dBi)	SBL_{max} (dB)	P_{f0}%	P_{SR1}	P_{SRH}	η_H %	η_S%	η_T %
$\chi = \{1\}$	Failure		−17.90	19.62	18.96	−3.62	−16.52	19.33	15.77	18.74	47.44	42.26	10.29	90.23	35.34	31.88
	Corrected	δ_n^c uniform	−19.68	20.36	19.06	−3.57	−19.45	18.86	15.68	−19.67	49.96	41.90	8.13	92.87	32.55	30.22
		δ_n^c variable	- 20.00	19.85	19.27	−3.70	−19.96	18.68	15.69	−21.30	50.82	41.67	7.50	92.50	32.44	31.00
$\chi = \{2\}$	Failure		−19.24	20.02	18.96	−3.42	−16.47	19.11	15.77	−19.25	47.44	42.25	10.30	90.41	35.61	32.19
	Corrected	δ_n^c uniform	−19.75	19.74	−3.53	19.29	−19.40	17.84	15.80	−17.70	50.65	41.88	7.46	93.94	34.95	32.83
		δ_n^c variable	−19.90	20.13	−3.74	19.23	−19.77	19.42	15.63	−23.78	50.42	41.35	8.22	91.77	34.99	32.11
$\chi = \{3\}$	Failure		−17.64	20.02	18.97	−3.59	−16.65	21.41	15.79	−19.32	47.40	41.09	10.27	90.40	35.43	32.02
	Corrected	δ_n^c uniform	−19.62	19.23	19.37	−3.68	−19.38	17.36	15.78	−20.61	50.57	42.32	7.11	92.62	38.22	35.39
		δ_n^c variable	−20.00	18.54	19.54	−3.77	−19.93	17.70	15.84	−23.24	51.41	42.55	6.04	93.55	36.61	34.25
$\chi = \{4\}$	Failure		−15.90	22.30	18.82	−3.59	−14.62	22.64	15.69	−19.09	46.98	41.76	11.26	89.78	34.43	30.91
	Corrected	δ_n^c uniform	−19.54	19.45	19.18	−3.64	−19.68	18.38	15.68	−20.19	50.33	41.61	8.06	92.41	35.44	32.75
		δ_n^c variable	−20.00	19.39	19.22	−3.69	−19.96	18.68	15.61	−23.84	50.31	41.57	8.11	91.89	36.05	33.12
$\chi = \{6\}$	Failure		−15.38	18.21	18.74	−3.43	−14.27	17.66	15.76	−19.22	45.82	42.44	11.74	88.48	33.51	29.64
	Corrected	δ_n^c uniform	−18.79	21.33	18.65	−2.7	−18.55	18.18	15.98	−18.97	46.45	46.81	6.73	96.26	25.70	24.73
		δ_n^c variable	−19.17	23.27	18.71	−3.42	−18.62	18.23	15.33	−18.34	50.08	42.06	7.86	92.02	26.81	24.67
$\chi = \{7\}$	Failure		−14.52	20.59	18.76	−3.49	−14.26	16.85	15.59	−18.37	46.24	42.10	11.65	88.45	33.11	29.28
	Corrected	δ_n^c uniform	−18.23	17.47	19.21	−3.01	−17.35	17.95	15.73	−19.36	53.54	41.67	4.79	95.70	25.40	24.30
		δ_n^c variable	−18.14	21.21	18.49	−3.05	−17.76	18.37	15.48	−15.22	47.82	43.23	8.95	91.05	24.62	22.42
$\chi = \{8\}$	Failure		−14.51	17.24	18.78	−3.52	−14.34	16.53	15.70	−19.13	46.51	41.93	11.55	88.52	33.09	29.29
	Corrected	δ_n^c uniform	−17.68	19.39	19.09	−3.87	−15.00	17.33	15.54	−18.39	53.20	42.30	4.49	95.51	24.98	23.85
		δ_n^c variable	−17.92	19.23	17.8	−2.22	−16.91	18.15	15.67	−12.10	39.17	45.39	15.43	85.20	22.34	18.03

https://doi.org/10.1017/S1759078722001179 Published online by Cambridge University Press

Table 3. Statistical analysis of the reconfigured antenna radiation pattern using different modulating pulse waves

Cases	Array status		f_0			f_1					P_{SR}%					
			SLL_0 (dB)	$FNBW_0$ (deg)	D_0 (dBi)	SBL_1 (dB)	SLL_1 (dB)	$FNBW_1$ (deg)	D_1 (dBi)	SBL_{max} (dB)	P_{f0}%	P_{SR1}	P_{SRH}	η_H %	η_S%	η_T %
$\delta_n^c = 0$	$\chi = \{6\}$	**Worst**	−16.38	25.55	17.41	−3.16	−16.35	22.33	14.64	−14.37	38.84	39.88	20.63	79.28	31.72	25.14
		Best	−18.35	23.27	17.72	−2.46	−17.91	19.39	15.08	−21.58	43.92	40.53	15.93	84.22	32.95	27.75
		Mean	−17.75	23.66	17.54	−2.72	−17.50	20.58	14.86	−16.45	40.75	40.24	19.00	81.43	31.49	25.64
		Variance	0.85	1.82	0.02	0.10	0.58	1.82	0.05	11.03	5.35	0.08	4.63	4.49	0.08	0.81
	$\chi = \{7\}$	**Worst**	−17.55	21.39	17.33	−2.60	−17.03	18.46	15.05	−12.55	37.33	39.37	22.86	77.73	30.17	23.45
		Best	−17.74	20.76	17.57	−2.32	−17.34	18.12	15.06	−13.31	39.17	39.80	21.45	79.88	32.73	26.14
		Mean	−17.67	21.19	17.42	−2.42	−17.24	18.31	15.05	−12.82	36.03	39.56	22.38	77.26	31.11	24.03
		Variance	0.01	0.07	0.01	0.01	0.02	0.02	0.00	0.12	0.55	0.02	0.38	0.37	0.44	0.41
	$\chi = \{8\}$	**Worst**	−16.41	20.13	17.03	−3.03	−15.18	18.00	15.20	−9.55	33.42	40.17	26.26	74.00	28.13	21.00
		Best	−17.42	18.60	18.07	−1.96	−16.54	16.99	15.39	−15.34	41.22	40.58	18.55	81.23	36.28	29.47
		Mean	−17.11	19.30	17.55	−2.48	−15.74	17.46	15.30	−12.14	37.24	40.39	22.37	78.66	32.81	25.80
		Variance	0.16	0.47	0.23	0.23	0.44	0.23	0.01	6.39	12.58	0.03	13.01	11.71	10.45	13.04
δ_n^c = uniform	$\chi = \{6\}$	**Worst**	−17.13	23.84	18.65	−4.17	−16.70	20.02	14.82	−11.72	46.45	39.21	6.73	93.23	20.11	18.75
		Best	−18.79	21.33	19.18	−2.7	−18.55	18.18	15.98	−21.14	57.78	46.81	3.01	97.51	25.40	24.76
		Mean	−17.98	22.17	19.01	−3.89	−17.50	18.95	15.42	−17.97	54.79	41.06	4.15	96.76	24.33	23.54
		Variance	0.37	0.98	0.04	0.45	0.50	0.57	0.19	21.23	22.03	10.43	2.18	1.64	4.61	5.41
	$\chi = \{7\}$	**Worst**	−17.57	22.35	18.67	−4.04	−16.13	18.46	15.24	−13.20	48.67	40.06	6.13	94.80	20.13	19.08
		Best	−18.23	19.45	19.21	−3.01	−17.55	16.90	15.76	−19.79	55.65	45.20	4.20	96.44	24.72	23.84
		Mean	−17.85	20.77	19.00	−3.77	−17.37	17.75	15.49	−17.86	53.75	41.49	4.74	95.62	23.59	22.55
		Variance	0.11	1.06	0.04	0.18	0.20	0.32	0.05	7.11	7.05	4.72	0.66	0.64	3.54	3.65
	$\chi = \{8\}$	**Worst**	−15.81	19.50	18.38	−4.38	−15.00	17.84	15.00	−11.25	44.94	37.54	8.19	92.21	17.98	16.57
		Best	−17.68	18.89	19.31	−2.62	−16.68	16.90	15.87	−21.85	57.86	46.88	4.17	96.60	27.28	26.35
		Mean	−17.32	19.28	18.99	−3.74	−15.55	17.31	15.69	−17.68	52.63	42.03	5.34	94.76	24.99	23.68
		Variance	0.26	0.63	0.34	0.73	0.76	0.12	0.05	37.26	36.78	6.93	14.28	11.35	20.32	23.11
δ_n^c = variable	$\chi = \{6\}$	**Worst**	−18.91	30.58	18.31	−3.47	−18.54	20.11	15.18	−14.37	45.41	41.90	10.51	89.34	24.71	22.07
		Best	−19.60	23.21	18.71	−2.79	−19.39	19.03	15.55	−18.34	50.68	44.50	7.43	93.60	26.22	24.54
		Mean	−19.32	24.91	18.49	−3.13	−18.89	19.57	15.39	−16.77	47.98	43.09	8.92	91.81	25.29	23.22
		Variance	0.08	10.09	0.03	0.09	0.14	0.21	0.02	3.74	5.53	1.20	1.81	2.58	1.05	1.27

(*Continued*)

Table 3. (*Continued.*)

Cases	Array status	f_0				f_1			P_{SR}%					
		SLL_0 (dB)	$FNBW_0$ (deg)	D_0 (dBi)	SBL_1 (dB)	SLL_1 (dB)	$FNBW_1$ (deg)	D_1 (dBi)	SBL_{max} (dB)	P_0%	P_{SR1}	P_{SRH}	η_H %	η_S%	η_T %
$\chi = \{7\}$	**Worst**	**−18.08**	20.53	18.44	−3.30	−16.97	18.15	15.34	−16.26	47.34	41.61	11.05	89.09	25.91	23.08
	Best	**−18.32**	21.22	18.65	−3.16	−17.47	18.01	15.49	−17.25	49.00	42.84	8.17	92.13	27.65	25.47
	Mean	**−18.26**	20.74	18.58	−3.23	−17.42	18.08	15.44	−16.74	48.28	42.37	9.35	91.42	26.03	23.79
	Variance	**0.01**	0.07	0.01	0.00	0.04	0.00	0.00	0.15	0.54	0.25	1.15	1.79	0.48	0.19
$\chi = \{8\}$	**Worst**	**−16.91**	20.02	17.79	−3.78	−15.03	18.15	15.30	−8.62	38.88	40.11	7.33	85.93	19.67	16.90
	Best	**−17.92**	17.92	19.07	−1.96	−17.23	17.21	15.89	−22.94	50.04	46.85	15.43	93.22	30.81	28.72
	Mean	**−17.37**	18.99	18.42	−3.00	−16.25	17.69	15.61	−15.65	45.13	43.54	11.32	88.55	25.61	22.68
	Variance	**0.25**	0.63	0.34	0.73	0.77	0.12	0.05	37.26	36.78	6.93	14.28	11.35	20.99	23.71

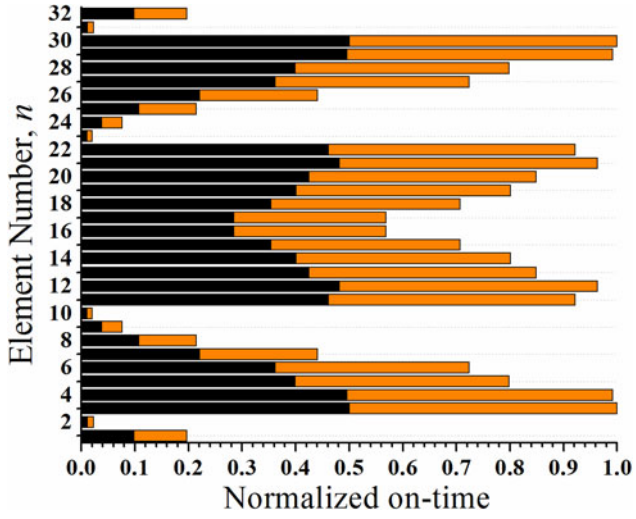


Fig. 9. DE-optimized pulse-switching sequence to synthesized reference sum flat-top patterns for a TMLA of $N = 32$ (Example 2).

can be reconciled with improved radiation characteristics in terms of improved directivity and reduced undesired sideband power loss.

Failure correction using trapezoidal pulse with non-uniform rise/fall time

Finally, the trapezoidal pulse-based switching with different values of δ_n^c for the individual pulse is applied to reconfigure the array patterns of the said failure array. Therefore, the optimization parameter vector for DE becomes $\mu^T = \{\xi_n^c, \vartheta_n^c, \delta_n^c\}$. The optimized switching parameters under case 1 and case 2 are shown in Figs 8(a) and 8(b), while the reconciled patterns are depicted in Figs 8(c) and 8(d), respectively. The radiation parameters of the corrected patterns are detailed in Table 1. Numerically, the achieved radiation parameters are as follows: SLLs at f_0 and f_1 are −19.27 and −19.47 dB for case 1 and that for case 2 are −19.46 and −19.27 dB; FNBWs are 20.30 and 18.66° for case 1 and 22.12 and 21.01° for case 2, respectively. The directivities of the patterns are 19 and 15.50 dBi for case 1 and 18.69 and 14.14 dBi for case 2. The overall efficiency of the TMA has been improved as compared to the rectangular pulse. It can be seen that only for the corrected pattern case 1, SLL_0 and D_0 are slightly less than that obtained with uniform pulse switching. However, as compared to the other cases, all other radiation parameters are improved. Further, the realized reconfigured patterns using this switching strategy are more closed to that of the original reference patterns with an enhanced directivity.

Element-wise statistical performances to correct the faulty pattern

Occurrence of element failure in antenna array is a random event and the amount of pattern degradation due to array failure depends on the position of the faulty elements on the array aperture. To observe the element-wise impact on array failure, the different radiation parameters of the pattern with array failure and that corresponding to the corrected pattern are presented in Table 2. As evidence from the reported literatures [20–27], it can be observed that the element failure toward the array edge has less influence on the pattern and the degraded pattern under such cases can be reconfigured closed to that of the original

https://doi.org/10.1017/S1759078722001179 Published online by Cambridge University Press

Table 4. Radiation performance of TMLA of $N = 32$, $d = \lambda/2$ (Example (2))

Array status		f_0				f_1				P_{SR}%					
		SLL_0 (dB)	$FNBW_0$ (deg)	D_0 (dBi)	SBL_1 (dB)	SLL_1 (dB)	$FTBW_1$ (deg)	R_d (dB)	SBL_{max} (dB)	P_{f0} %	P_{SR1}	P_{SRH}	η_H %	η_S %	η_T %
$\chi = 0$		−18.77	13.35	20.18	−4.60	−19.38	41.08	0.497	−20.47	42.16	35.17	22.65	77.34	28.17	22.98
$\chi = \{2,29\}$		−18.15	13.40	20.13	−6.33	−16.85	41.44	1.224	−14.26	42.54	35.35	22.07	67.92	26.30	17.86
Corrected	i.$\delta_n^c = 0$	−18.82	18.26	19.76	−4.72	−20.01	40.84	0.500	−19.57	45.43	36.07	18.48	81.51	24.11	19.65
	ii.δ_n^c = uniform	−19.13	12.44	20.98	−4.92	−19.85	44.68	0.499	−20.62	55.79	35.52	8.68	91.32	26.04	23.78
	iii.δ_n^c = variable	−23.82	13.43	20.94	−4.64	−20.18	43.21	0.500	−20.88	58.80	32.80	8.40	93.17	26.33	24.53

failure free pattern. On the other hand, the element failure near the center elements strongly effects the pattern and the proposed method can be used to correct the same with little compromisation of SLL. It also shows that, compared to the rectangular pulse, the trapezoidal pulse is more effective for multi-pattern failure correction, as it reduces the discrepancy between failure-free pattern and reconfigured pattern more than rectangular one. Nonetheless, the trapezoidal pulse of uniform rise/fall time is found to be efficient in suppression of undesired harmonic power than the trapezoidal pulse of variable rise/fall time (δ_n^c).

By taking some random faulty elements, the statistical performances for correcting the pattern with different modulating pulse waves are presented in Table 3. For each case, after running the algorithm 20 times; the best, worst, mean, and variance of different radiation parameters are calculated. The presented results indicate that the proposed failure correction method with less variance is efficient to steadily reconfigure the pattern at each trial run.

Example 2: failure correction of dual-beam TMLA with sum-flattop pattern

The optimized switching sequence to synthesize the desired dual patterns as mentioned previously is shown in Fig. 9. Let, the array is disrupted with failure of two elements as $\chi = \{2, 13\}$ as considered in [24]. The radiation parameters of both the failure-free and failure patterns are listed in Table 4. The results show that, due to failure, both the patterns at f_0 and f_1 are distorted. For the sum pattern, SLL and FNBW are increased and directivity is decreased. For the flat-top pattern, SLL, FNBW as well as ripple factor are increased.

The optimized pulse sequences of the corrected patterns under the three strategies are shown in Figs 10(a)–10(c). The corresponding corrected patterns along with the failure-free and the failure patterns at f_0 and f_1 are presented in Figs 11(a) and 11(b) respectively. The obtained radiation parameters of the three strategies are mentioned in Table 4. Though by using rectangular pulse-switching strategy, the both SLLs of the corrected dual patterns are matched with the failure-free pattern, a significant amount of power ($P_{SRH} = 18.48\%$) is wasted at higher order harmonic radiation, while the power at the desired frequencies, f_0 and f_1 are $P_{f0} = 45.43\%$ and $P_{SR1} = 36.07\%$ respectively.

On the other hand, with respect to the rectangular pulse, the use of trapezoidal pulse switching with uniform δ_n^c improves SLL and directivity of the reconfigured pattern at f_0 by 0.31 and 1.22 dBi. Moreover, with respect to the rectangular pulse switching, P_{SRH} is reduced by 9.8% while P_{f0} and overall efficiency are increased by 10.36 and 4.13% respectively.

Finally, it is worth to note that by using the pulse switching with non-uniform δ_n^c, the SBL_{max} is reduced to −20.88 dB with the significant suppression of P_{SRH} to 8.40%. Consequently, the power at the desired harmonics is improved with the values of $P_{f0} = 58.80\%$ and $P_{SR1} = 32.80\%$. Thus, most of the radiated power is concentrated to reconstruct the desired patterns. The use of 32 number of SPST switches reduces the switching efficiency largely as compared to the 16-element TMA of Example 1. The results presented in Tables 1 and 2 show that, though with the application of the trapezoidal pulse the used harmonic power efficiency is improved by reducing power losses in the unused harmonics, the overall efficiency is some-what degraded because of the relatively smaller values of the switching efficiency in synthesizing the desired patterns. This efficiency can be

https://doi.org/10.1017/S1759078722001179 Published online by Cambridge University Press

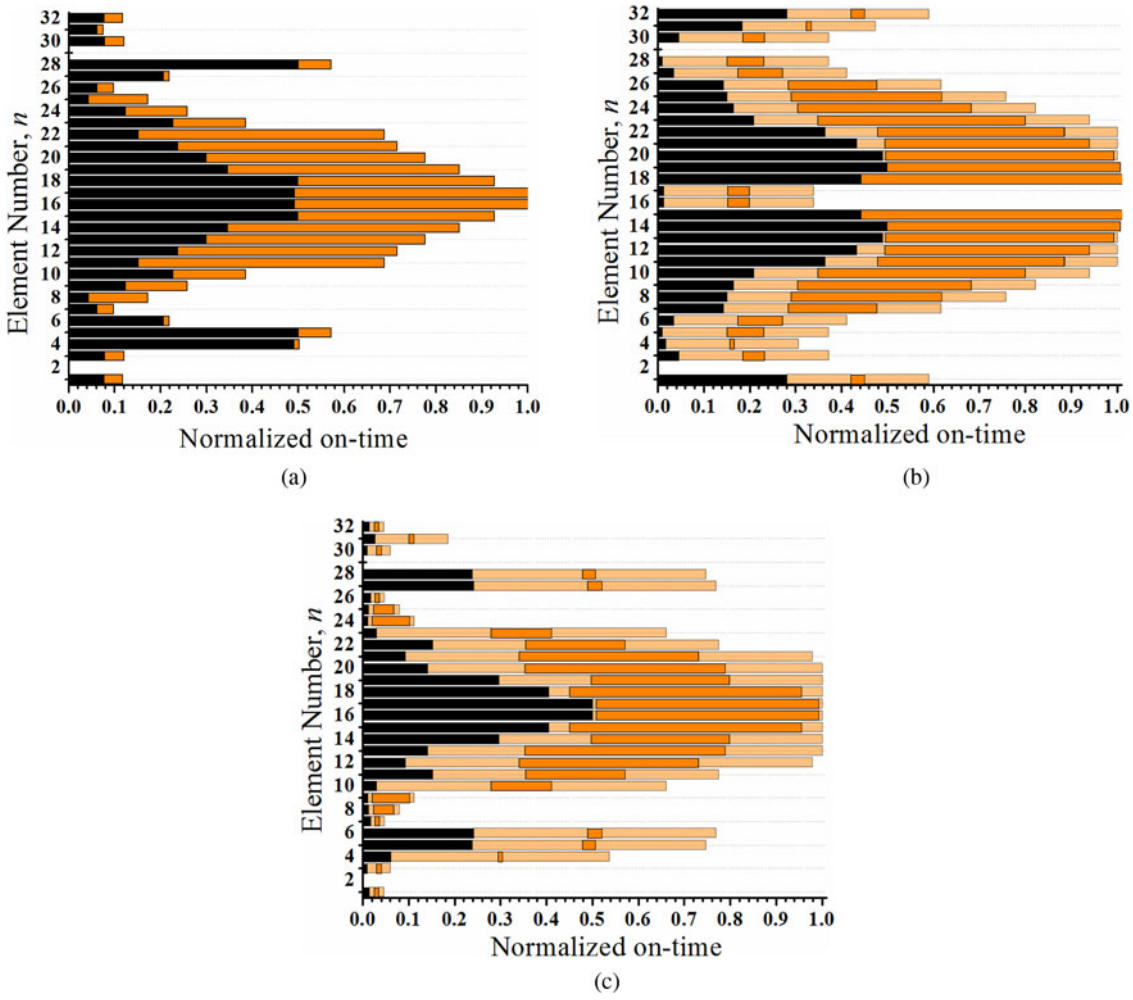


Fig. 10. DE-optimized corrected pulse-switching sequence for a TMLA of $N = 32$ (Example 2) considering ($\chi = \{2, 29\}$). (a) Rectangular with zero rise/fall time ($\delta_n^c = 0$). (b) Trapezoidal with uniform zero rise/fall time ($\delta_n^c = \delta_0^c$). (c) Trapezoidal with variable rise/fall time (δ_n^c).

improved by reducing the number of switches by applying SPDT switch or sub-arraying method.

For completeness, a comparative convergence characteristic curve of DE to reconfigure the failure patterns under the three different switching strategies is depicted in Fig. 12. Also, the power radiation at different sidebands is calculated and their variations at different harmonics are depicted in Fig. 13. The figures clearly show that as compared to rectangular pulse, the cost

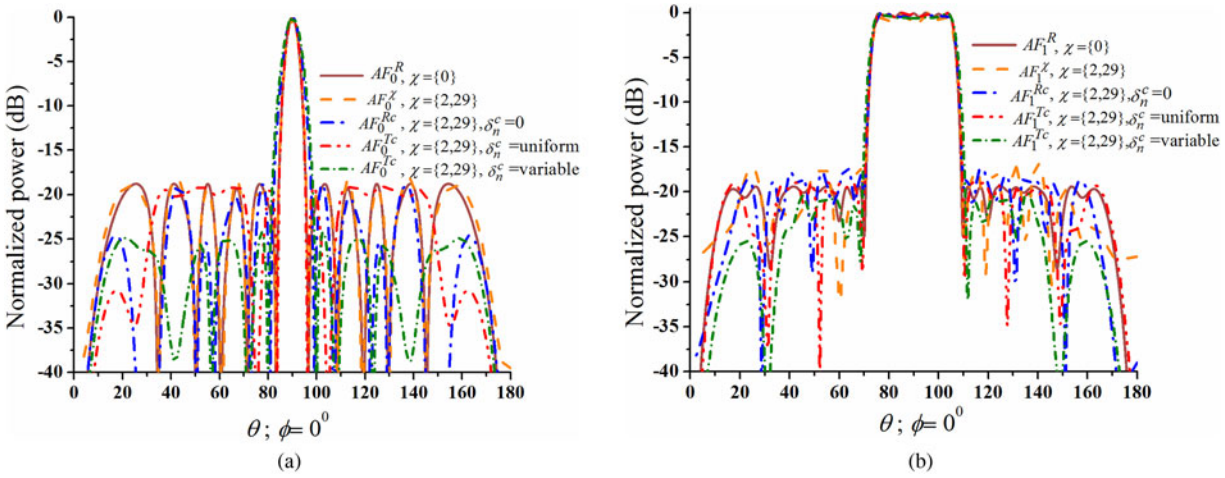


Fig. 11. DE-optimized reconstructed synthesized sum flat-top patterns for a TMLA of $N = 32$ (Example 2) considering ($\chi = \{2, 29\}$) (a) at f_0 and (b) at f_1.

https://doi.org/10.1017/S1759078722001179 Published online by Cambridge University Press

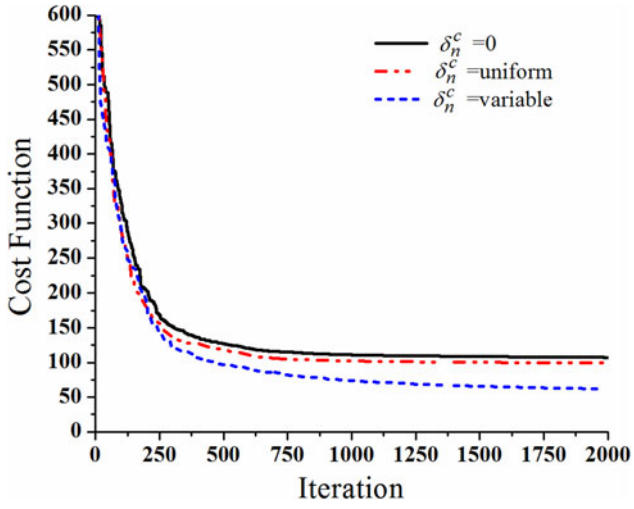


Fig. 12. Comparative convergence characteristic curves of DE-optimized pattern reconfiguration using shaped pulse of different rise/fall times with $\chi = \{2, 29\}$ in a 32-element TMLA.

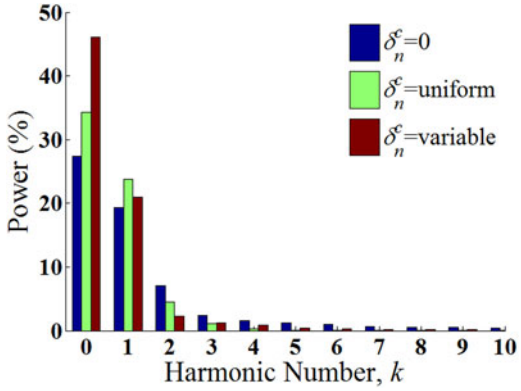


Fig. 13. Relative sideband radiation for $k \in [1, 10]$ of DE-optimized pattern reconfiguration using shaped pulse of different rise/fall times with $\chi = \{2, 29\}$ in a 32-element TMLA.

function value as well as the higher order sideband power for both the trapezoidal pulses are lower. The lower cost function values in the convergence curve indicate that the reconstructed patterns are more closed to satisfy the desired requirements. However, the reduction of higher order sideband power leads to provide more power to produce the desired patterns. Hence, the performance of the trapezoidal pulse-switching strategy to correct the degraded patterns under failure condition is better than the conventional rectangular pulse-switching strategy. While two trapezoidal pulse-switching strategies are compared, it is to be noted that the pulse switching with non-uniform rise/fall time increases the number of optimizing variables, particularly because of non-uniform values of δ_n^c for the individual elements; however, it provides more diversity in the search space of the stochastic optimization algorithm. As a result, with non-uniform rise/fall time, both cost function value and higher sideband power are less as compared to that with uniform rise/fall time. This clearly depicts that the trapezoidal pulse with non-uniform rise/fall time is best suited to correct the degraded patterns in the presence of element failure.

Conclusion

The trapezoidal pulse-shaping strategy by using rise/fall time as an additional degree of freedom is adopted for simultaneous pattern reconfiguration at fundamental and harmonic frequency in the presence of element failure in TMLA. In this regard a closed form expression of the harmonic power radiated by the proposed half wavelength TMLA fed by shifted trapezoidal pulse is derived. It is found from the numerical study that the rectangular pulse of zero rise/fall time is not well motivated for pattern reconfiguration as it does not provide the optimum directivity by simultaneously maintaining the SLL and SBL. The trapezoidal pulse provides additional flexibility to reconfigure the degraded patterns closed to the failure-free reference patterns by significantly suppressing the higher order harmonic power. The trapezoidal pulse-switching strategy is found to be efficient for pattern correction in the presence of element failure by improving the directivity and reducing the undesired higher order harmonic power losses. Further, practically it is difficult to realize rectangular pulse with exactly zero rise/fall time. Whereas the trapezoidal pulse of finite rise/fall time has the flexibility in controlling the time-slope of the ON-OFF switching states. In this aspect, the trapezoidal pulse-switching scheme also has the advantage of practical realization with desired parameters of the required pulse.

Acknowledgement. This work is financially supported by the Ministry of Electronics and Information Technology (MeitY), Govt. of India under Visvesvaraya Young Faculty Fellowship of Visvesvaraya Ph.D. scheme (Grant No. PhD-MLA-4(29)/2015-16) and the work is under DST-SERB project Ref. file number EEQ/2016/00836, dated January 17, 2017.

Conflict of interest. None.

References

1. **Kummer W, Villeneuve A, Fong T and Terrio F** (1963) Ultra-low sidelobes from time-modulated arrays. *IEEE Transactions on Antennas and Propagation* **11**, 633–639.
2. **Mukherjee A, Mandal SK and Ghatak R** (2019) Differential evolution to synthesize low sidelobe thinned isophoric time-modulated planar array with increased directivity. *International Journal of RF and Microwave Computer-Aided Engineering* **29**, e21938.
3. **Bregains JC, Fondevila-Gomez J, Franceschetti G and Ares F** (2008) Signal radiation and power losses of time-modulated arrays. *IEEE Transactions on Antennas and Propagation* **56**, 1799–1804.
4. **Mandal S and Mandal SK** (2019) Harmonic power losses in time-modulated arrays with non-uniform period modulation. *AEU–International Journal of Electronics and Communications* **108**, 45–52.
5. **Yang S, Gan YB and Tan PK** (2004) Evaluation of directivity and gain for time-modulated linear antenna arrays. *Microwave and Optical Technology Letters* **42**, 167–171.
6. **Mandal SK, Ghatak R and Mahanti GK** (2011) Minimization of side lobe level and side band radiation of a uniformly excited time modulated linear antenna array by using Artificial Bee Colony algorithm, *2011 IEEE Symposium on Industrial Electronics and Applications*, pp. 247–250.
7. **Yang S, Gan YB, Qing A and Tan PK** (2005) Design of a uniform amplitude time modulated linear array with optimized time sequences. *IEEE Transactions on Antennas and Propagation* **53**, 2337–2339.
8. **Zhang SR, Zhang YX and Cui CY** (2020) Efficient multiobjective optimization of time-modulated array using a hybrid particle swarm algorithm with convex programming. *IEEE Antennas and Wireless Propagation Letters* **19**, 1842–1846.
9. **Bekele ET, Poli L, Rocca P, Urso MD and Massa A** (2013) Pulse-shaping strategy for time modulated arrays – analysis and design. *IEEE Transactions on Antennas and Propagation* **61**, 3525–3537.

https://doi.org/10.1017/S1759078722001179 Published online by Cambridge University Press

10. **Yao A, Wu W and Fang D** (2015) Single-sideband time-modulated phased array. *IEEE Transactions on Antennas and Propagation* **63**, 1957–1968.
11. **Li H, Chen Y and Yang S** (2021) Design and analysis of an amplitude-phase weighting module for harmonic beamforming in time-modulated antenna arrays. *AEU – International Journal of Electronics and Communications* **138**, 153835.
12. **Farzaneh S and Sebak A** (2006) A novel amplitude-phase weighting for analog microwave beamforming. *IEEE Transactions on Antennas and Propagation* **54**, 1997–2008.
13. **Poli L, Rocca P, Oliveri G, Chuan M, Mazzucco C, Verzura S and Lombardiet R** (2018) Advanced pulse sequence design in time-modulated arrays for cognitive radio. *IEEE Antennas and Wireless Propagation Letters* **17**, 898–902.
14. **He C, Chen Q, Cao A, Chen J and Jin R** (2019) Application of the time modulated array in satellite communications. *IEEE Wireless Communications* **26**, 24–30.
15. **Shan C, Ma Y, Zhao H and Shi J** (2018) Joint radar-communications design based on time modulated array. *Digital Signal Processing* **82**, 43–53.
16. **Mandal SK, Mahanti GK and Ghatak R** (2014) Synthesis of simultaneous multiple-harmonic-patterns in time-modulated linear antenna arrays. *Progress In Electromagnetics Research (PIER) M* **34**, 135–142.
17. **Patnaik A, Choudhury B, Pradhan P, Mishra RK and Christodoulou C** (2007) An ANN application for fault finding in antenna arrays. *IEEE Transactions on Antennas and Propagation* **55**, 775–777.
18. **Rodriguez-Gonzalez JA, Ares-Pena F, Fernandez-Delgado M, Iglesias R and Barro S** (2009) Rapid method for finding faulty elements in antenna arrays using far field pattern samples, *2009 3rd European Conference on Antennas and Propagation*, pp. 3380–3384.
19. **Mukherjee A, Mandal SK and Ghatak R** (2021) Efficient computational method for fast extraction of faulty elements from multipattern time-modulated arrays. *IEEE Transactions on Antennas and Propagation* **69**, 1982–1991.
20. **Acharya OP, Patnaik A and Sinha SN** (2014) Limits of compensation in a failed antenna array. *International Journal of RF and Microwave Computer-Aided Engineering* **24**, 635–645.
21. **Acharya OP and Patnaik A** (2017) Antenna array failure correction [antenna applications corner]. *IEEE Antennas and Propagation Magazine* **59**, 106–115.
22. **Peters TJ** (1990) A conjugate gradient based algorithm to minimize the peak sidelobe level of planar arrays with element failures. *International Symposium on Antennas and Propagation Society, Merging Technologies for the 90's* **2**, 848–851.
23. **Migliore MD, Pinchera D, Lucido M, Schettino F and Panariello G** (2015) A sparse recovery approach for pattern correction of active arrays in presence of element failures. *IEEE Antennas and Wireless Propagation Letters* **14**, 1027–1030.
24. **Beng-Kiong Y and Yilong L** (1999) Array failure correction with a genetic algorithm. *IEEE Transactions on Antennas and Propagation* **47**, 823–828.
25. **Grewal NS, Rattan M and Patterh M** (2012) A linear antenna array failure correction using firefly algorithm. *Progress in Electromagnetics Research M* **27**, 241–254.
26. **Poli L, Rocca P, Oliveri G and Massa A** (2014) Failure correction in time-modulated linear arrays. *IET Radar, Sonar & Navigation* **8**, 195–201.
27. **Malhat H, Zainud-Deen A, Rihan M and Badawy M** (2022) Elements failure detection and radiation pattern correction for time-modulated linear antenna arrays using particle swarm optimization. *Wireless Personal Communications* **125**, 2055–2073.
28. **Rocca P, Masotti D, Costanzo A, Salucci M and Poli L** (2017) The role of accurate dynamic analysis for evaluating time-modulated arrays performance. *IEEE Antennas and Wireless Propagation Letters* **16**, 2663–2666.
29. **Masotti D, Poli L, Salucci M, Rocca P and Costanzo A** (2019) An effective procedure for nonlinear dynamic optimization of time-modulated arrays. *IEEE Antennas and Wireless Propagation Letters* **18**, 2204–2208.
30. **Aksoy E and Afacan E** (2012) Calculation of sideband power radiation in time-modulated arrays with asymmetrically positioned pulses. *IEEE Antennas and Wireless Propagation Letters* **11**, 133–136.
31. **Zeng Q, Yang P, Lin H, Yang F and Yang S** (2021) Generalized closed-form sidebands' radiation expressions for 4-D antenna arrays. *IEEE Transactions on Antennas and Propagation* **69**, 1193–1197.
32. **Zeng Q, Yang P, Yin L, Lin H, Wu C, Yang F and Yang S *et al.*** (2021) Calculation of the total radiated power for 4-D antenna arrays with arbitrary time modulated waveform. *IEEE Transactions on Antennas and Propagation* **69**, 9015–9020.
33. **Chen Q, Zhang J, Wu W and Fang D** (2020) Enhanced single-sideband time-modulated phased array with lower sideband level and loss. *IEEE Transactions on Antennas and Propagation* **68**, 275–286.
34. **Maneiro-Catoira R, Brégains J, García-Naya JA and Castedo L** (2019) Time-modulated phased array controlled with nonideal bipolar squared periodic sequences. *IEEE Antennas and Wireless Propagation Letters* **18**, 407–411.
35. **Paul CR** (2006) *Introduction to Electromagnetic Compatibility*, 2nd Edn. Hoboken, NJ: Wiely.
36. **Aksoy E** (2014) Calculation of sideband radiations in time-modulated volumetric arrays and generalization of the power equation. *IEEE Transactions on Antennas and Propagation* **62**, 4856–4860.
37. **Poli L, Rocca P, Manica L and Massa A** (2010) Pattern synthesis in time-modulated linear arrays through pulse shifting. *IET Microwaves, Antennas & Propagation* **4**, 1157–1164.
38. **Storn R and Price K** (1997) Differential evolution – a simple and efficient heuristic for global optimization over continuous spaces. *Journal of Global Optimization* **11**, 341–359.
39. **Qing A and Lee CK** (2010) *Differential Evolution in Electromagnetics*. Spinger, Verlag Berlin Heidelberg.

Appendix

Since the Fourier coefficient a_{nk}^T is a complex quantity, the product of $\sum_{\substack{k=-\infty \\ k\neq 0}}^{\infty} a_{mk}^T a_{nk}^{T*}$ for $m = n$ can be written as [30],

$$\sum_{\substack{k=-\infty \\ k\neq 0}}^{\infty} a_{nk}^T a_{nk}^{T*} = 2\sum_{k=1}^{\infty} |a_{nk}^T|^2 = \frac{1}{2}\frac{1}{\pi^4 \delta_n^{T^2}} \sum_{k=1}^{\infty} \frac{(1-\cos 2\pi k\xi_n^T)(1-\cos 2\pi k\delta_n^T)}{k^4}$$
$$= \frac{1}{2}\frac{1}{\pi^4 \delta_n^{T^2}} \left[\sum_{k=1}^{\infty} \frac{1}{k^4} - \sum_{k=1}^{\infty} \frac{\cos 2\pi k\xi_n^T}{k^4} - \sum_{k=1}^{\infty} \frac{\cos 2\pi k\delta_n^T}{k^4} + \frac{1}{2}\sum_{k=1}^{\infty} \frac{\cos 2\pi k(\xi_n^T + \delta_n^T)}{k^4} + \frac{1}{2}\sum_{k=1}^{\infty} \frac{\cos 2\pi k(\xi_n^T - \delta_n^T)}{k^4} \right]. \quad \text{(A1)}$$

https://doi.org/10.1017/S1759078722001179 Published online by Cambridge University Press

Now cosidering the identity of fourth-order Riemann's Zeta function as given below [9],

$\sum_{k=1}^{\infty}(\cos kx/k^4) = (\pi^4/90) - (\pi^2x^2/12) + (\pi x^3/12) - (x^4/48)$ with$0 \le x \le 2\pi$, the final step of (A1) is obtained as,

$$\xi_n^T(1-\xi_n^T) - \frac{\delta_n^T}{3}. \tag{A2}$$

Similarly, for $m \neq n$,

$$\sum_{\substack{k=-\infty \\ k\neq 0}}^{\infty} a_{mk}^T a_{nk}^{T*} = 2\sum_{k=1}^{\infty} a_{mk}^T a_{nk}^{T*} = \frac{1}{4}\frac{1}{\pi^4\delta_m^T\delta_n^T}\left[\begin{array}{l} \sum_{k=1}^{\infty}\frac{(\cos \pi k\{(\xi_m^T-\xi_n^T)+(\delta_m^T-\delta_n^T)\})}{k^4} + \sum_{k=1}^{\infty}\frac{(\cos \pi k\{(\xi_m^T-\xi_n^T)-(\delta_m^T-\delta_n^T)\})}{k^4} \\ -\sum_{k=1}^{\infty}\frac{(\cos \pi k\{(\xi_m^T-\xi_n^T)+(\delta_m^T+\delta_n^T)\})}{k^4} - \sum_{k=1}^{\infty}\frac{(\cos \pi k\{(\xi_m^T-\xi_n^T)-(\delta_m^T+\delta_n^T)\})}{k^4} \\ -\sum_{k=1}^{\infty}\frac{(\cos \pi k\{(\xi_m^T+\xi_n^T)+(\delta_m^T-\delta_n^T)\})}{k^4} - \sum_{k=1}^{\infty}\frac{(\cos \pi k\{(\xi_m^T+\xi_n^T)-(\delta_m^T-\delta_n^T)\})}{k^4} \\ +\sum_{k=1}^{\infty}\frac{(\cos \pi k\{(\xi_m^T+\xi_n^T)+(\delta_m^T+\delta_n^T)\})}{k^4} + \sum_{k=1}^{\infty}\frac{(\cos \pi k\{(\xi_m^T+\xi_n^T)-(\delta_m^T+\delta_n^T)\})}{k^4} \end{array}\right] \tag{A3}$$

$$= \left[\overline{\xi_{mn}^T} - \xi_m^T\xi_n^T - \frac{\overline{\delta_{mn}^T}}{3}\right]. \tag{A4}$$



Ananya Mukherjee (Student Member IEEE) received B.Tech. from West Bengal University of Technology (WBUT) in the year 2011. She completed her M.Tech. in Telecommunication Engineering from National Institute of Technology Durgapur in 2014 and received Ph.D. degree from the same institute in September 2022. Her research interest lies in the application area of antenna array synthesis and design through time-modulation using evolutionary algorithms.



Sujoy Mandal (Student Member IEEE AP-S, MTT Society) received the B.Tech. degree in Electronics and Communication Engineering from West Bengal University of Technology (WBUT), Kolkata, India in 2013, and M.Tech. degree in Microwave Engineering from The University of Burdwan, Burdwan, West Bengal, India in 2016. Presently, he is pursuing the Ph.D. degree from the National Institute of Technology (NIT) Durgapur, Durgapur, India. His research interest includes the analysis and synthesis of the radiation characteristics of time-modulated antenna arrays, prototype development of time-modulated arrays, algorithm development to obtain the precise position solution in multiple global navigation satellite systems (multi-GNSS) constellations, and the development of GNSS based cost-effective applications.



Sujit Kumar Mandal (Member IEEE) received the B.Sc. degree in Physics Honours from the University of Calcutta in 2001. He completed B.Tech. and M.Tech. in Radio Physics and Electronics from the Institute of Radio Physics and Electronics, C. U. in the years 2004 and 2006 respectively. He received the Ph.D. degree in January 2014 from the National Institute of Technology (NIT), Durgapur where he is an Assistant Professor in the Department of Electronics and Communication Engineering, since 2010. He has published more than 50 research papers in various national and international peer-reviewed journals and conferences. His present research area includes application of soft computing techniques in antenna array optimization, time-modulated antenna arrays, microstrip patch antenna, RF energy harvesting, and on-chip antenna design.



Rowdra Ghatak (Member IEEE) initiated his career in microwave engineering as a trainee with the CEERI Pilani, Pilani, India, in the domain of fabrication and testing of S-band magnetrons. Thereafter, he served at the National Institute of Science and Technology, Berhampur, and The University of Burdwan. He is currently a Professor with the Electronics and Communication Engineering Department, National Institute of Technology Durgapur, Durgapur, India. He has more than 250 publications in various national/international journals and conferences. His research interests include in the areas of fractal antenna, metamaterials, and application of evolutionary algorithms to electromagnetic optimization problems, RFID, and computational electromagnetic and microwave passive and active circuit design. Dr. Ghatak was a recipient of the URSI Young Scientist Award in 2005. He also received support under the DST Young Scientist scheme for the development of UWB radiating systems for imaging RADAR. He has served in various selection as well as project review committees in the state as well as in the national domain. He has also served as a reviewer for a NPTEL course on antennas. He is a member of the board of studies at UG and PG level at various state and central universities. He is also serving as a Research Advisor to the TCS Research in the domain of mmWave radio design and radiating systems.

https://doi.org/10.1017/S1759078722001179 Published online by Cambridge University Press